An experimental study of the influence of stress history on fault slip during injection of supercritical CO_2

Robert J. Cuss, Andrew C. Wiseall, Elena Tamayo-Mas, and Jon F. Harrington,

British Geological Survey, Keyworth, Nottingham, NG12 5GG, UK

Corresponding author: R.J. Cuss, British Geological Survey, Keyworth, Nottingham, NG12 5GG, UK (rjcu@bgs.ac.uk)

The injection of super-critical CO_2 into a depleted reservoir will alter the pore pressure of the basin, which if sufficiently perturbed could result in fault slip. Therefore, knowledge of the acceptable pressure limits is required in order to maintain fault stability. A two-part laboratory study was conducted on fully saturated kaolinite fault gouge to investigate this issue. Previously, we showed that fault slip occurred once pore-pressure within the gouge was sufficient to overcome the normal stress acting on the fault. For kaolinite, this behaviour occurred at a pressure similar to the yield stress. The current study shows that following a slow-reduction in the maximum principal stress, as would be expected through changes in effective stress, the reactivation pressure shows a stress memory. Consequently, the pressure necessary to initiate fault slip is similar to that required at the maximum stress encountered. Therefore, fault slip is at least partially controlled by the previous maximum stress and not the current stress state. During the slow reduction in normal stress, the flow characteristics of the fault remain unchanged until pore-pressure exceeds shear stress and does not increase significantly until it exceeds normal stress. This results in fault slip, which slows the rate of flow increase as shear is an effective self-sealing mechanism. These observations lead to the conclusion that stress history is a vital parameter when considering fault stability.

Keywords

Fault slip; Carbon Capture and Storage; kaolinite; shear testing; stress memory.

1.0 Introduction

The capture of CO_2 from large point source emitters and storage in the form of a super-critical fluid within geological formations has been identified as a key technology in tackling anthropogenic climate change (Haszeldine, 2009; Bickle, 2009). To achieve a reduction in emissions, significant quantities of CO_2 need to be injected into suitable geological formations capable of containing the fluid for thousands of years, such as active or depleted hydrocarbon reservoirs, and saline aquifers. Several Carbon Capture and Storage (CCS) demonstration projects have been conducted injecting megatonne scale CO_2 into geological reservoirs, such as Sleipner (saline aquifer; Norwegian North Sea; Arts *et al.*, 2008), Weyburn (enhanced oil recovery; Saskatchewan Province, Canada; Wilson and Monea, 2004) and In Salah (enhanced gas recovery; Algeria; Mathieson *et al.*, 2010). Faults are usually present in potential CCS sites and this paper aims to investigate how CCS operations may impact fault-slip potential. Perturbations of the reservoir pore fluid pressures are necessary to utilise storage capacity. These changes in pore pressure, and as a result the stress state, may result in undesired geomechanical deformation that could affect the integrity of the overlying seal and any faults present.

An existing fault will remain locked as long as the applied shear stress is less than the frictional and cohesive strength of the contact. Karl Terzaghi first showed in 1923 that pore-fluid under pressure has a profound effect on the physical properties of porous solids (Terzaghi, 1943). In a saturated porous system, the fluid supports some proportion of the applied load, and lowers the overall stress exerted through the grains. Strength is therefore determined not by confining pressure alone, but by the difference between confining and pore-pressures. Hubbert & Rubey (1959) showed that this behaviour applies to faults, so that a pore pressure of P_f reduces the frictional strength of faults (τ_f), which can be represented by a criterion of Coulomb form:

$$\tau_f = C + \mu\sigma_n' = C + \mu(\sigma_n - P_f) \qquad [1]$$

where C is the cohesive strength of the fault, μ is the coefficient of friction, σ_n is the normal stress on the fault, and $'$ denotes effective stress. Byerlee (1978) showed that μ ranges between 0.6 and 1.0 for most rocks, but can be approximated as 0.75 ± 0.15 (Sibson, 1994). However, phyllosilicate minerals can have a significantly lower coefficient of friction, e.g. 0.1 – 0.32 for smectite (Morrow *et al.*, 1992; Saffer & Marone, 2003), 0.35 – 0.68 for illite (Morrow *et al.*, 1982, 1992; Saffer & Marone, 2003), ~0.3 for wet kaolinite (Crawford *et al.*, 2008) and up to 0.8 for dry kaolinte (Morrow *et al.*, 2000). Fault reactivation can occur when shear stress along the fault (τ) equals τ_f. This condition can occur through an increase in shear stress, decrease in normal stress, or an increase in fluid pressure. Additionally, chemical interactions between fault gouge and CO_2 saturated brine can result in clay alteration to weaker minerals, which will result in a change in frictional behaviour that could result in fault movement. Further, the variation in frictional properties with saturation state for kaolinite could result in fault weakening if water migrates into an under-saturated fault core where the mineral is present.

Hydraulic and mechanical interactions therefore play a critical role in reactivating faults at various scales in the Earth's upper crust (Scholz, 1990). Injection of fluid and the resulting changes in the stress-state can result in the reactivation of existing faults if the pore pressure variation is sufficient in magnitude (Cappa & Rutqvist, 2011; Segall & Rice, 1995), which may result in seismic failure. This effect has occurred in geothermal projects (e.g. Bachmann *et al.*, 2012; Gan & Elsworth, 2014), waste water injection during shale gas exploration (e.g. Ellsworth, 2013), slip of an existing fault at Preese Hall (England) as a result of hydraulic stimulation (e.g. Clarke *et al.*, 2014; Holland, 2013), and by natural gas injection at the Castor storage site in Spain (Cesca *et al.*, 2014). However, only micro-seismicity has been observed during Carbon Capture and Storage (Verdon *et al.*, 2013).

Experimental work related to slip and/or fault reactivation has tended to look at mechanical controls using analogue sand-box experiments (Krantz, 1991; Richard & Krantz, 1991; Dubois *et al.*, 2002; Bellahsen & Daniel, 2005; Del Ventisette *et al.*, 2006) or examining the flow properties of fault gouge and inferring fault weakness on geomechanical response (Crawford *et al.*, 2008; Faulkner & Rutter, 2000; Faulkner & Rutter, 2001). Modelling studies of fault reactivation potential, or slip tendency, have been conducted by several workers; as summarised by Rutqvist (2012).

1.1 Objectives and previous work

This paper presents results from an experimental study aimed at evaluating the role of stress history on fault-slip potential within the laboratory. The current study represents the third stage of a three-part investigation of the potential for fault slip during the sequestration of carbon dioxide. The three parts of the study were; 1) the role of stress history on fault-flow properties, as reported in Cuss *et al.* (2016); 2) quantification of fault-slip potential as a result of elevated pore pressure, as reported in Cuss & Harrington (2016); and 3) the role of stress history on fault slip (the current study). The scenario being investigated is for a fault that has undergone a reduction in the maximum principal stress (vertical stress) through a change in effective stress, with an increase in pore pressure initiating fault slip. Therefore, an increase in pore pressure is directly simulated in response to the injection of CO_2. The objectives of the study are:

- Investigate the change in fault transmissivity during shear and/or reduction in stress;
- Investigate the pore-pressure necessary to initiate fault slip following a reduction in the maximum principal stress.

To simulate a critically stressed fault, gouge material was sheared to a stress representative of the residual shear strength, following which, vertical stress was reduced and finally pore pressure was elevated. The shearing of the fault to residual stress conditions ensured that the fault plane was actively stressed. The primary aim of the study was to establish the maximum pore pressure perturbations that could be employed during carbon sequestration on faults that have had a complex geological history.

Previous experimental work at the British Geological Survey (BGS) on fracture transmissivity in Opalinus clay (Cuss *et al.*, 2011; 2014[a,b]), Callovo-Oxfordian claystone (Cuss *et al.*, 2017) and kaolinite gouge (Sathar *et al.*, 2012) showed that hydraulic flow is a complex, focused, transient property that is dependent upon stress history, normal stress, shear displacement, fracture topology, fluid composition, and clay swelling characteristics. Cuss *et al.* (2016) showed that fault transmissivity has clear hysteresis during unloading, demonstrating that stress history is a vital component in dictating the flow properties of faults. Cuss & Harrington (2016) showed that fault slip occurred at a pressure dependent on the physical properties of the fault gouge, with different gouges showing variations in fault slip potential. The current experimental program aimed to extend this knowledge by investigating the influence of stress-history on the potential for fault slip.

2 Experimental setup

All experiments were performed using the bespoke Angled Shear Rig (ASR, Fig. 1) designed and built at the British Geological Survey. Previous experiments conducted on Opalinus Clay (Cuss *et al.*, 2009; 2011; 2014[b]) showed that fracture topology is a key parameter in controlling fluid flow along fractures. To reduce the number of variables required to fully understand flow and slip potential, an analogue discontinuity with smooth fracture surfaces was investigated. The surfaces of the discontinuity were machined from steel and therefore flow could only occur through the fault gouge within the discontinuity.

The ASR (Fig. 1) has five key components:

1. Rigid steel body that had been designed to have a bulk modulus of compressibility and shear modulus approximately two orders of magnitude greater than the clay gouge tested, resulting in minimal deformation of the apparatus compared to the test sample;
2. Vertical load system comprising an Enerpac hydraulic ram that was controlled using a Teledyne/ISCO 260D syringe pump, a rigid loading frame and an upper thrust block (up to 20 MPa vertical stress, 72 kN force). The Enerpac ram had a stroke of 105 mm, which means that it could easily accommodate the vertical displacement of the top block as it rides up the fault surface at constant vertical load. Note: The vertical stress created by the ram is not equal to the normal stress perpendicular to the fault plane and represents the maximum principal (vertical) stress within a reservoir;
3. Shear force actuator comprised of a modified and horizontally mounted Teledyne/ISCO 500D syringe pump designed to drive shear as slow as 14 microns a day at a constant rate (equivalent to 1 mm in 69 days), or as fast as 0.5 mm per second, along a low friction bearing. This capability gives a range of shear strain rate of more than 7 orders of magnitude;
4. Pore pressure system comprising a Teledyne/ISCO 500D syringe pump that could deliver either water or gas up to a pressure of 25.8 MPa. The syringe pump delivered fluid through the centre of the top block directly to the fault surface;
5. A state-of-the-art custom designed data acquisition system using National Instruments LabVIEW™ software facilitating the remote monitoring and control of all experimental parameters.

The experimental fault assembly consisted of precision machined 316 stainless steel top and bottom blocks (thrust blocks) with a dip of 30 degrees with respect to horizontal (the shearing direction). Previous workers (e.g. Crawford *et al.*, 2008; Tembe *et al.*, 2010) employed roughened surfaces to ensure slip was not simply between the clay gouge and thrust blocks. However, the thrust blocks used in the current study were polished so as not to introduce preferential pathways for flow. The top block was connected to the vertical loading arrangement by means of a swivel mechanism, which was engaged to the shoulders on either side of the top block. Care was taken in the design of the swivel mechanism so as to negate rotation and tilting of the top blocks and shear mechanism. Two pore pressure transducers, attached to ports that were positioned orthogonally to each other at 15 mm from the central pore fluid inlet allowed measurement of pore pressures within the fault gouge (Fig. 1a). The thrust blocks of the apparatus were made with a contact area of 60 mm × 60 mm. The lower thrust block was longer and wider than the top one so that the contact area of the experimental discontinuity could be maintained constant throughout the test. The movement of the top block relative to the bottom block was minimised to 1 mm (< 1.5 % shear strain) so that no adverse effects were caused by new clay gouge entering the fault at the leading edge of the top block and sheared clay gouge exiting at the trailing end of the thrust block.

As shown in a

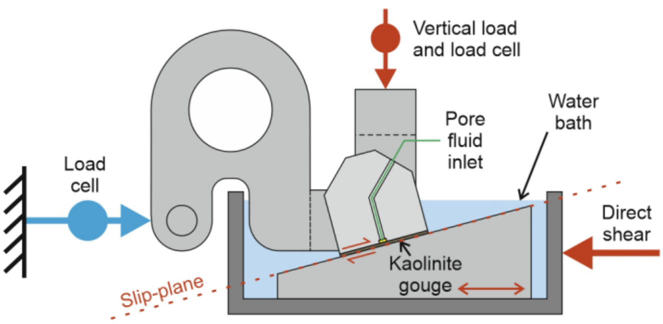

b

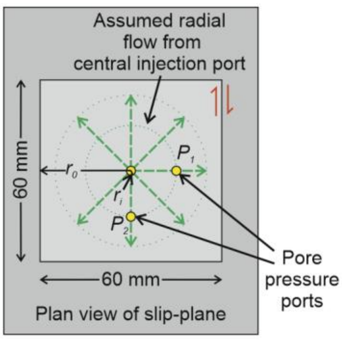

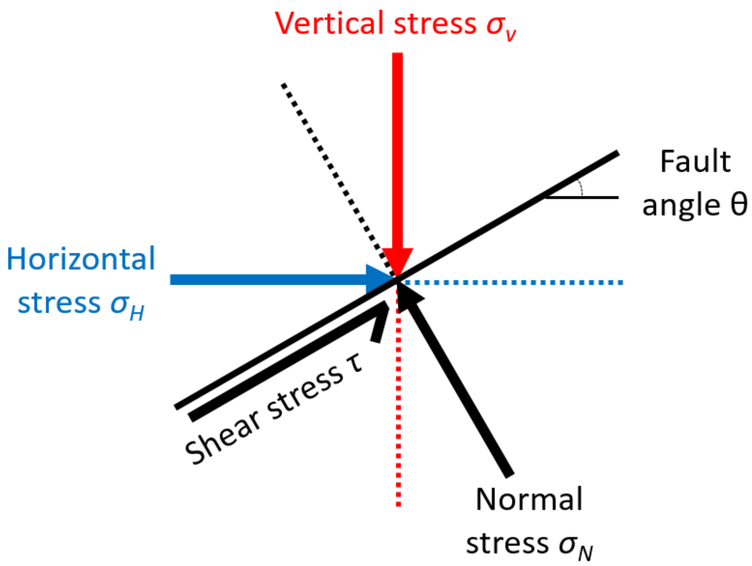

c

Figure 1a, the shear-force actuator acted upon the angled bottom-block of the apparatus. The movement of the bottom-block was measured using a linear variable differential transducer (LVDT), which had a full range of ± 25 mm and an accuracy of 0.5 µm. Vertical travel of the thrust block was measured by a high precision non-contact capacitance displacement transducer, which had a full range of ± 0.5 mm and an accuracy of 0.06 µm. Horizontal load was measured using a load cell fitted laterally to the top-block. This measured the force resultant from lateral movement of the bottom block transmitted through the clay gouge.

Kaolinite was selected as the gouge material for a number of reasons. Pure mechanical tests could not be conducted without gouge as the stainless steel thrust blocks would have cold-welded together. A synthetic lubricant could have been used, although this would not be representative of natural faults. Therefore, it was necessary to include a realistic gouge, with a clay-based material representing a faulted caprock. However, swelling clays such as illite and smectite add a significant complication to the interpretation of experimental results. The swelling can take several weeks to equilibrate and the injection of water risks further swelling if the clay gouge is not fully saturated. Therefore, kaolinite was selected as it has a minimal tendency to swell, yet displays many of the properties associated with clay gouge. The water content of the kaolinite gouge was such that it was fully saturated in order to minimise swelling resultant from water injection. Kaolinite is also a fault gouge observed in nature and has been used by a number of previous investigators (e.g. Crawford *et al.*, 2008).

Gouge material for the experiments was prepared from powdered kaolinite, supplied by Imerys from St Austell (UK). Highley (1984) report that kaolinite is of well-ordered form with coarse hexagonal platelelets. The equivalent spherical diameter of the clay grains was 100 % (by weight) less than 10 μm, 95 % less than 2 μm, and 85 % less than 1 μm. Water (16 ± 0.1 g of de-ionised water) and clay powder (20 ± 0.1 g) were stirred for five minutes giving a fully saturated paste. The mixed paste was smeared uniformly onto the surface of the top block, which was carefully lowered onto the bottom block thus forming a paste gouge. The initial thickness of the gouge was about 1 mm. However, as no lateral confinement was made of the clay gouge, thickness decreased to approximately 180 ± 10 μm with loading up to 10 MPa. The excess clay squeezed from between the thrust blocks acted as a buffer preventing water from the shear bath entering the fault gouge or causing sloughing. No lateral gouge confinement was included because sealing elements with a high frictional component would have been required along the fault surface, which would have experimentally overshadowed the low frictional properties of the clay. However, the thickness of the gouge was seen to be sufficient as the minimum thickness experienced (180 μm) is much greater than the grain size of the kaolinite used (95 % less than 2 μm).

Eight experiments were conducted that looked at aspects of the role of stress history on flow properties and/or fault reactivation pressure (Table 1). These tests examined the effects of instantaneous reduction in vertical stress before reactivation pressure was determined, the change in fracture transmissivity during the slow reduction of vertical stress to almost zero vertical stress, and a gradual reduction in vertical stress before reactivation pressure was determined. In addition, envelopes for starting, yield, and peak shear stress were determined for all 28 tests conducted as part of the current study and additional tests reported in Cuss & Harrington (2016). The experimental programme was designed to examine aspects of changes of effective stress during injection of carbon dioxide and the period following injection, as well as the role stress history during geological time-scales prior to injection would have on the mechanical strength of faults.

All tests were conducted in multiple stages, the first of which was identical. Once the apparatus had been assembled, vertical stress was increased in steps up to the desired magnitude and a constant pore pressure was established in the clay gouge. Vertical stress was kept constant by the Teledyne/ISCO syringe pump for the remainder of the stage. The shear actuator was initiated to give 1 mm of strain over a 24-hour period, which equated to a strain-rate of 1.93×10^{-7} s^{-1}. Data were logged every minute throughout the experiment. During the 24-hour shear stage, the gouge had achieved stable-peak stress sliding. After approximately 24 hours, the shear actuator was turned off and the next stage was conducted.

For tests ASR_BigCCS_21Kfl and ASR_BigCCS_34Kfl (Table 1) the Teledyne/ISCO syringe pump controlling vertical stress was switched to constant refill mode, which resulted in a slow and gradual reduction of vertical stress acting on the fracture. Pore-fluid flow was monitored until a condition of very low vertical stress after approximately 48 hours. For tests ASR_BigCCS29Ksh – ASR_BigCCS_33Ksh (Table 1) the second stage of testing was a slow reduction in vertical stress over a 24-hour period followed by a stage of fault reactivation. For test ASR_BigCCS_20Kst (Table 1) an instantaneous stepped reduction in vertical stress was performed, followed by a stage of fault reactivation.

The fault reactivation stage was performed by injecting de-ionised water into the central port of the top thrust block at a constant flow-rate of 0.25 ml h^{-1}, which was sufficient to raise pore fluid pressure within the fault gouge to 10 MPa over a 24-hour period. Fault reactivation was observed as an instantaneous reduction in horizontal stress and simultaneous change in vertical displacement of the load frame. Some tests showed single movements, others showed multiple slip events, whilst some tests (see Table 1) showed no evidence of reactivation. Still minimal reactivation was possible, causing changes in shear stress and vertical displacement that were too small to measure.

Once the time of fault reactivation was known, it was possible to determine the vertical and horizontal stress at reactivation. Pore pressure was calculated as the average pore pressure within the fault gouge, which was more representative of the force acting to oppose normal stress over the complete fracture surface as opposed to the pump injection pore pressure that represented a localised increase over the area of the injection filter. As shown in Figure 1a, radial flow was assumed from the central injection filter, giving an average pore pressure within the gouge of 0.35 Pp, where Pp is the injection pressure. The recorded vertical and horizontal stress components were rotated to represent normal and shear stress, as represented in Figure 1b. Throughout this paper, vertical and horizontal stresses are referred to when discussing far-field stresses, whereas normal and shear stress are used to discuss the local stress on the fault.

3 Experimental results

The initial stages of all experiments were performed in a similar manner (Fig 2a). Tests were mostly conducted at 4.9 MPa normal stress for a constant vertical stress of 6.0 MPa, although test ASR_BigCCS_33Ksh was conducted at a reduced 2.0 MPa normal stress for a 2.5 MPa vertical stress. As shown in Figure 2a, good repeatability was seen during repeat testing at given normal stresses. Test ASR_BigCCS_29Ksh had a slightly reduced shear modulus, but achieved similar peak shear strength conditions (Figs. 2a, c).

The coefficient of friction (μ) for all tests was calculated as the ratio between normal stress and differential shear stress, where the differential shear stress is equal to the difference between the peak stress and the starting shear stress (Figs 2b, 3). Figure 2b shows that μ ranges between 0.26 and 0.28 for the kaolinite tested, which yields a friction angle of 15.1º and a fault angle of 37.5º. As seen, the test conducted at a lower normal stress (ASR_BigCCS_33Ksh) gave a similar coefficient of friction. This outcome compares well with that reported by Crawford *et al.* (2008) of 0.3 for 100 % kaolinite given the limited strain conducted in the current study. Therefore, we infer that our shear box apparatus gives similar results to the more traditional triaxial method of investigating fault behaviour. It should be noted that μ could be estimated as the slope of the peak stress (Fig. 3), which would give a result of 0.85, which corresponds well with the result published by Morrow *et al.* (2000) for dry kaolinite. However, the kaolinite tested was fully saturated and wet.

Figure 2c shows an example result for test ASR_BigCCS_31Ksh and the four parameters that can be calculated for each test. The starting shear stress is simply the magnitude of stress observed before shear was initiated. The initial stress-strain response was linear, and the slope is used to calculate the shear modulus. In most tests, the deviation from this linear response occurred at the yield shear stress as the departure from the linear region by 0.02 MPa. All tests were checked to determine that this criterion was appropriate and that a similar result would have been achieved by manual identification. The final shear stress parameter identified was peak shear stress. As shown in Figure 2a, all tests showed classic elasto-plastic behaviour. Therefore, the peak stress condition also describes the residual strength of the gouge, although a complete peak was not fully achieved by the end of the limit of 700 µm displacement (1.3 % shear strain). Table 1 states the directly measured horizontal and vertical stress for the start, yield, and peak shear stress conditions, along with the corresponding normal and shear stress.

Figure 3 shows the results for starting, yield, and peak shear stresses for all experiments in the current study and those reported in Cuss & Harrington (2016). As can be seen, the data describe linear relationships with few outliers. Linear regression is shown in Figure 3 with the intercept set to zero. An example shear test is also displayed showing the variation of both normal and shear stress during the active shearing of the gouge.

Figure 4 summarises the observations made of fracture transmissivity during shearing. For test ASR_BigCCS_30Ksh, a marked reduction in fracture transmissivity (*T*) was noted with shear. Initially, T was 6.6×10^{-15} m^2 s^{-1} and reduced to a steady value of 2.1×10^{-17} m^2 s^{-1}. A slight increase in flow can be inferred at yield when the clay gouge would have undergone dilatancy, although the noise in the data does not provide conclusive evidence. This test suggests that shearing reduces fracture transmissivity by two orders of magnitude. In contrast, quite dissimilar results were seen in test ASR_BigCCS_34Kfl. From the onset of the shear stage, flow within the fracture was low, averaging a steady transmissivity of 1.9×10^{-17} m^2 s^{-1}. Yield of the fault gouge is expected to include a degree of dilatancy on the fault plane, which is likely to enhance fluid flow. However, this behaviour was not observed even though the fluid injection pressure was greater than the shear stress acting on the fault plane. Therefore, it can be concluded that in this test shear had no effect on fracture transmissivity. However, the flow rate throughout the shear stage was similar to that achieved after 200 μm of shear in test ASR_BigCCS_30Ksh.

Following the shear stage, the syringe pump controlling the vertical stress was changed to refill mode to slowly lower the vertical stress. Figure 5 summarises the mechanical response recorded by the data. As can be seen, all tests followed a stress path parallel with the envelope defined for peak shear stress of kaolinite. For test ASR_BigCCS_34Kfl, which was unloaded to almost zero vertical stress, a minor curvature of the unload path was seen (Fig. 5c). Here, the difference between the observed shear stress during unload and the envelope for peak stress is shown. This non-linear response may be derived from hysteresis in the gouge or may suggest that the envelops for starting, yield and peak shear stress are not perfectly linear.

Figure 6 shows the fracture transmissivity response of the fault gouge during slow unloading over a 2-day period. Both normal and shear stress showed some hysteresis during unload (Fig. 6a), with pore fluid pressure exceeding normal stress within 1.5 days of unload. Initially, fracture transmissivity was low (Fig. 6b), with an average around 2.0×10^{-17} m^2 s^{-1}, and no discernible change until day 4.34, when a small variation in normal displacement was observed (Fig. 6c) along with a minor change in shear stress (Fig. 6c). This variation is approximately when the average pore fluid pressure in the gouge equalled the shear stress. Flow accelerated at day 4.6 and 4.64 when marked changes in normal displacement and shear stress were observed. This behaviour shows a marked change in the ratio of shear stress to normal stress (Fig. 6b). The coincidental change in normal displacement and shear stress indicates that fault slip was initiated. By day 4.6, the average pore pressure in the fault gouge had exceeded the normal stress acting on the fault plane. A second event occurred at day 4.75 with a similar change in normal displacement, shear stress, and shear stress to normal stress ratio. However, this event coincides with a reduction in the rate of increase of fracture transmissivity. This change suggests that the second fault slip, or reactivation, resulted in a degree of self-sealing of the gouge, whereas the first enhanced flow. Fracture transmissivity continued to increase until day 5.07 when at a fracture transmissivity of approximately 690×10^{-17} m^2 s^{-1}, the gouge underwent breakthrough and could no longer support fluid pressure. This event corresponded to a change in normal displacement and shear stress of greater magnitude than the previous events, which can be described as a catastrophic slip.

Figure 7 shows an example result from fault reactivation test ASR_BigCCS_31Ksh using de-ionised water as the injection fluid. As shown (Fig. 7a), the injection of fluid at a constant rate increased the pore fluid pressure in the fault from the starting average pore pressure of 0.1 MPa up to 4 MPa over a 7-hour period. As pore pressure rose, a single slip event was initiated, as shown by a reduction in shear stress (Fig. 7b) and change in vertical displacement (Fig. 7c).

This occurred at an average pore pressure within the gouge of 3.05 MPa. No further slip events were detected in this test, whereas some tests showed multiple slip events.

Figure 8 summarises the fault-slip data following vertical stress reduction, as would occur during uplift and erosion of a sedimentary basin over geological timescales prior to injection. As shown in Figure 8 and Table 1, three of the five tests showed fault slip. These events occurred at an average pore pressure between 2.73 and 3.82 MPa. They are clearly at a pressure much greater than the peak shear-stress condition for kaolinite. Comparing these data following stress reduction, with the fault-slip data reported in Cuss & Harrington (2016) shows an increase in fault slip pressure. In Cuss & Harrington (2016), it was concluded that fault slip of a critically stressed fault would occur at a pressure close to the yield strength of the gouge. The current data show that following stress reduction, the fault can sustain a much greater pore pressure, similar in magnitude to that expected at the maximum stress condition experienced (Table 1).

Test ASR_BigCCS_20Kst (Fig. 8, open blue circle) with its vertical stress reduced in an instantaneous step following shearing has a contrasting result. The stress state for fault slip is similar to that expected had the reduced vertical stress been the maximum stress condition.

4 Discussion

Figure 4 shows that shear may influence the flow properties of faults. For test ASR_BigCCS_30Ksh, a clear reduction in flow was observed as the fault started to shear, with up two orders of magnitude reduction in transmissivity during active shearing of the kaolinite fault gouge. However, the story is not clear-cut, as shown in Figure 4b. Test ASR_BigCCS_34Kfl showed little or no response to shearing. To determine the true behaviour, it is useful to compare the current studies using the analogue fault arrangement with those conducted on competent rocks, such as reported for Opalinus clay, a Jurassic shale from

Switzerland (Cuss *et al.*, 2011; 2014[a,b]). Cuss *et al.* (2014[a]) showed that shear had a profound influence on fracture transmissivity. During the initial stages of shearing, one order of magnitude reduction in flow was seen, while attaining a transmissivity similar to the host rock. Opalinus clay has a composition of 40 – 80 % clay (9 – 29 % illite, 3 – 10 % chlorite, 6 – 20 % kaolinite, and 4 – 12 % illite/smectite mixed layers in the ratio 70/30), other minerals (15 – 30 % quartz, 6 – 40 % calcite, 2 – 3 % siderite, 0 – 3 % ankerite, 1 – 7 % feldspars, 1 – 3 % pyrite, <1 % organic carbon) and a total water content ranging from 4 – 19 % (Gautschi, 2001). Microstructural analysis attributed the reduction of flow to clay smearing along the fracture reducing the overall fracture aperture. Unfortunately, the use of saturated clay gouge in the current tests do not allow for the recovery of the test material at the end of the test, and therefore it is not possible to make any microstructural observations. However, it is suggested that the reduction seen during testing can only be attributed to shearing. The transmissivity seen in the tests that did not show any change in flow (ASR_BigCCS_34Kfl; 1.9×10^{-17} m^2 s^{-1}) is of similar magnitude to that seen in the test that showed flow reduction (ASR_BigCCS_30Ksh; 2.1×10^{-17} m^2 s^{-1}). Therefore, it is suggested that during the setup of the tests, a small shear occurred during the increase in vertical stress prior to initiating shear. During setup, a small vertical stress is imposed on the gouge and checks are made that the top thrust block is not touching the side of the apparatus, as this would severely affect results. At this time, it is common to adjust the position of the top thrust block and this action results in the gouge undergoing small amounts of shear prior to the start of the test. Further evidence of the self-sealing capacity of shear in kaolinite is the observed change in transmissivity during the reduction in maximum principal stress test (ASR_BigCCS_34Kfl). In this test, at low vertical stresses, the fracture transmissivity started to increase. At a stress state where fault slip was initiated, the rate of change of flow reduced. Therefore, shear reduced the transmissivity of the fault gouge.

The vertical stress reduction test (ASR_BigCCS_34Kfl, Fig. 6) shows that the slow change in normal stress did not result in recovery of transmissivity between day 3.1 and day 4.3, with transmissivity remaining less than 10×10^{-17} m^2 s^{-1}. This behaviour matches the observation reported in Cuss *et al.* (2016[a]), where flow did not recover in the stepped approach undertaken until vertical stress was very low. The current data shows that transmissivity did not start to increase until the average pore pressure in the fault was greater than the normal stress on the fault. At this condition, small changes in the shear stress and vertical displacement were observed as fluid started to flow. Therefore, shear stress acting on the fault dictates when flow started to recover. Fluid is not able to increase its ability to flow until the pressure exerted exceeds the minimum principal stress component, i.e. the shear stress. This behaviour helps to explain the hysteresis seen in the system during stress reduction.

During test ASR_BigCCS_34Kfl, fault slip was not initiated until the average pore pressure within the fault gouge exceeded the normal stress acting on the fault. Therefore, slip occurs once the normal component of stress, created by the pore fluid pressure, exceeds the opposing normal stress. Consequently, stress-history on fault slip could be inferred to have no influence and that the magnitude of transmissivity and slip is simply dictated by the timing of when pore fluid pressure exceeds shear or normal stresses. However, the tests conducted following a reduction in normal stress showed a response that was not simply based on pore pressure overcoming normal stress, but rather the occurrence of clear stress memory (Fig. 8). The pore pressure required to cause slip following normal stress reduction is of a similar magnitude to that expected at the maximum stress encountered. For example, as shown in Table 1, test ASR_BigCCS_31Ksh was initially loaded to a normal stress of 5.84 MPa, which as shown by Cuss & Harrington (2016) would predict a slip pressure of 3.93 MPa. During unloading the normal stress was reduced to 2.67 MPa, which would predict a slip pressure of 1.68 MPa. The slip pressure was recorded to be 3.05 MPa, which is nearly twice that expected had the fault only been stressed to a maximum of 2.67 MPa and is less than that expected had the slip test been conducted at the maximum normal stress of 5.84 MPa. Although a small reduction did occur, it is clear that slip occurs at a pore pressure significantly greater than that seen at the current stress state. This behaviour can in part be explained by the non-recovery of flow seen in the gouge. The hysteresis seen in the transport properties is mirrored in the non-recovery of the mechanical properties. However, test ASR_BigCCS_34Kfl showed that normal and shear stresses are recovered during vertical stress reduction and it would be expected that this shows a recovery in mechanical properties. Therefore, it can be suggested that the maximum stress encountered results in a repacking of the kaolinite grains. The reduction of vertical stress results in the elastic recovery of stress, but the pore throats of the re-packed kaolinite do not recover. This textural change gives the gouge a memory of the maximum stress encountered. This outcome is not overly surprising as many factors of clay-rich rocks, such as mechanical strength and flow properties, are related to the over-consolidation ratio, which is directly related to the maximum stress-state that the rock has encountered during geological history (Burland, 1990; Skempton, 1970; Horseman *et al.*, 1987).

One test was performed with an instantaneously stepped reduction in normal stress (ASR_BigCCS_20Kst). The resultant slip pressure for this test corresponded with what was expected had the reduced normal stress of 2.5 MPa been the maximum stress encountered. Therefore, the instantaneous, stepped, reduction in vertical stress appears to have "re-set" the stress-memory of the fault. It should be noted that only one test was conducted with a stepped reduction in vertical stress. This observation requires further exploration and is outside of the scope of the current study. It is unlikely that this phenomena is derived from drainage of the kaolinite gouge, as even at the low fracture transmissivity recorded, the pore pressure in the gouge is quick to equilibrate.

Figure 9 shows the results from the current study plotted in the Mohr space for stress history test ASR_BigCCS_33Ksh (Fig. 9a) and vertical stress reduction flow test ASR_BigCCS_34Kfl (Fig. 9b). The stress history test shows that at the maximum stress state, the fault was far from the condition necessary to result in slip. The slow reduction in vertical stress did not bring the stress state to a condition of slippage and hence no movement was observed. Fault slip was initiated by raising pore fluid pressure, but as can be seen, movement occurred at a pressure much greater than the Mohr approach would have predicted. This error in the Mohr approach is created by the analysis not taking into account the stress history of the fault. The flow test conducted until the fault was fully exhumed (test ASR_BigCCS_34Kfl), shows that the high pore pressure used in this test (5 MPa) still resulted in an initial condition of stability. The reduction in vertical stress resulted in failure of the fault at a stress condition greatly below that predicted by the Mohr analysis. Again, this outcome is a result of the simple analysis not including stress history. Therefore, it can be concluded that the widely accepted Mohr analysis of fault reactivation becomes problematic when the fault under consideration has undergone a complex stress-history. When such a history is the case, the stress history has to be incorporated.

Careful consideration needs to be taken with respect to the time component when interpreting the current experiments, which were conducted over a short duration. The initial shearing stage lasted approximately 24-hours, the slow reduction of stress took a further 24 hours, while the final pore-pressurisation stage took up to 24 hours. All three stages were undertaken considerably faster than would occur in the natural or man-made systems of interest. Considering unloading during exhumation and erosion over geological history prior to injection, the event could take millions of years, eight orders of magnitude slower than the current experiments. Considering a stress change based on an engineering time scale of 10 years would be four orders of magnitude slower. During pressurisation, the time-scale of pressure increase is likely to range between a month to a few years, therefore representing a pressure rise 2 to 3 orders of magnitude slower. It should also be noted that the magnitude of the pore pressure perturbation is likely to be much less than encountered during the current experiments. In designing the experiments, a 24-hour period was determined as a trade-off between the time necessary for the clay gouge to drain and the total time available for all experiments. Despite the low fracture transmissivity of $< 5 \times 10^{-17}$ m^2 s^{-1}, the small surface area of the experimental apparatus (60 × 60 mm) drained relatively quickly. For instance, the tests operated at 0.25 MPa pore pressure would take approximately 1 – 2 hours for the pressure to reduce and plateau once the injection syringe pump was turned off. Therefore, drainage is not a major limitation of the test methodology. However, over geological and engineering time-scales, processes may act that would alter this behaviour. For example, slow compaction and consolidation of the gouge material may alter the cohesion of the fault plane, which will alter the slip potential. However, this change is likely to strengthen the fault gouge and lead to an enhanced stress memory effect as slip pressure would increase. The current study clearly identified a stress memory effect of slip potential common with the hysteresis seen in flow properties in a stress-reducing system (e.g. Cuss *et al.*, 2016). Further work is required to investigate this feature for realistic rocks and natural conditions to verify the observations. Such experiments would aim to investigate the influence of other geological processes that may occur, such as compaction and clay smearing, on the potential for fault slip. Accounting for all the limitations of the current experimental investigation, stress memory in flow and slip potential still requires further attention.

The main implication of the current work is that a consideration only of the current stress-state will result in inaccurate predictions of flow and fault slip potential. For the flow properties, not accounting for stress history will result in the over-estimate of flow. Therefore, the faults will be over-estimated for their ability to transmit fluids. In terms of fault slip, not accounting for stress-history will result in the under-prediction of the pore pressure necessary to initiate fault reactivation. Consequently, faults that have a significant stress-history prior to injection will be stronger than predicted and may sustain a greater pore pressure variation. It should be noted that exhumation and erosion of overlying sediments prior to injection is not the only possible driver for stress variation in a reservoir used for carbon sequestration. Localised variations will result from pore-pressure variations, thermally derived stresses resultant from injection cooling, or from stresses resultant from reservoir compaction. These stress drivers are all likely to result in relatively minor changes in the stress-state acting on faults and may not result in noticeable stress-memory. The inaccurate prediction in flow is not so straightforward. Whilst it will result in faults appearing to be better seals than predicted, it will result in the under-estimation of pore fluid pressure under a sealing fault, which could result in higher pore-fluid pressures acting upon the fault and/or caprock. This latter observation suggests that stress-history should not be ignored if pore pressures are likely to get close to the magnitude that would either cause fault slip or new failure. Stress history is also important to understand the flow properties of all faults to yield an understanding of the fluid distribution within a reservoir during injection.

The hysteresis seen in flow and mechanical behaviour in clay-rich rocks is well established in engineering geology and is one of the basic concepts of critical-state soil mechanics (Roscoe *et al.*, 1958; Schofield & Wroth, 1968). However, such phenomena are not routinely incorporated into structural geological studies that are based on rock mechanics, which in general defines driving forces and not relaxing stress-states. Several studies have looked at geological history, and hence stress history, such as Rutter *et al.* (2012) who aimed to unravel the stress history of the Carboneras fault zone. However, this study did not result in stress history predictions of the faults themselves. Aldrich *et al.* (1991) examined the stress history of a geothermal site in Honduras. By unravelling the regional stress fields from the faults, they were able to examine the stress field and potential for reactivation of faults during hydraulic fracturing for geothermal energy. Whilst the magnitude of stress change was not determined, their work clearly showed the influence of stress history on the fault system. Several studies have looked at slip potential or reactivation (e.g. Morris *et al.*, 1996; Gartrell *et al.*, 2002; Colletini *et al.*, 2005; Moeck *et al.*, 2009). However, none incorporate the hysteresis seen in flow and mechanical behaviour observed during the current study. A future study could be conducted for an existing, or future, reservoir identified for sequestration of carbon dioxide to reconstruct the full stress history that all faults have experienced. Flow modelling could then be used to determine the full consequence of the observations from the current study and those of Cuss & Harrington (2016). This approach will establish whether stress history on faults plays a significant role on fluid flow within the reservoir and the influence it has on slip potential.

5 Conclusions

This paper presents results from an experimental study of eight shear tests on a simulated fault angled 30° to the shear direction with a fault gouge of saturated kaolinite. The primary aim of the study was to investigate the influence of stress-history on fault slip by comparing the current data with that of Cuss & Harrington (2016). The main conclusions of the study were:

- The injection of pore-fluid into a depleted reservoir could result in fault slip if the pore pressure perturbation is sufficient.
- Following a slow reduction in the maximum principal stress, the pore pressure necessary to initiate fault slip has a clear memory, with slip occurring at a pressure similar to that observed at the maximum stress condition.
- Ignoring stress-history can result in an under-estimate of the pore pressure necessary to initiate fault reactivation.

- The stress “memory” observed is suggested to be created by the re-packing of the clay gouge, which occurs at the maximum stress condition.
- The instantaneous reduction in vertical stress results in fault slip and a resetting of the stress memory. This is an unlikely scenario during storage of CO_2.
- Shear has been observed to be an effective self-sealing mechanism during the initial stages of shearing and also following fault slip.
- Fault transmissivity remains unchanged during the slow reduction in the maximum principal stress until the average pore pressure exceeds the shear stress (minimum principal stress). Fault slip is not triggered until average pore pressure exceeds the normal stress on the fault.
- The Mohr analysis of fault reactivation is not sufficient to predict when fault reactivation is likely to occur because stress history is not included.
- Stress-history is a vital parameter in determining both fault transmissivity and fault slip potential. Not accounting for stress history will result in an under-estimate of the maximum pore pressure that can be achieved in a reservoir. However, ignoring stress-history will result in an under-estimate of fault transmissivity that may result in higher than predicted pore pressure in the vicinity of faults, which if sufficient, could result in slip. Therefore, it is concluded that stress-history should be considered fully when assessing reservoirs for the storage of CO_2.

Acknowledgements

The study was undertaken by staff of the Minerals and Waste Program of the BGS using the experimental facilities of the Transport Properties Research Laboratory (TPRL). The authors would like to thank the two anonymous reviewers and editor William Dunne who's suggestions greatly improved this paper. We thank skilled staff of the Research & Development Workshops at the BGS, in particular Humphrey Wallis, for their design and construction of the experimental apparatus. This publication has been produced with support from the BIGCCS Centre. The BIGCCS Centre is part of the Norwegian research programme Centres for Environment-friendly Energy Research (FME) and is funded by the following partners: ConocoPhillips, Gassco, Shell, Statoil, TOTAL, Engie and the Research Council of Norway (193816/S60). The BGS authors publish with the permission of the Executive Director, British Geological Survey (NERC).

References

Aldrich,. M.J., Adams, A.I., and Escobar, C. (1991) Structural geology and stress history of the Plataneres geothermal site, Honduras: implications on the tectonics of the northwestern Caribbean plate boundary. Journal of Volcanology and Geothermal Research, 45, 59-69.

Arts, R.J., Chadwick, R.A., Eiken, O., Thibeau, S., and Nooner, S. (2008) Ten years' experience of monitoring CO_2 injection in the Utsira Sand at Sleipner, offshore Norway. *First Break*, **26**, pp.65–72.

Bachmann, C.E., Wiemer, S., Goertz-Allmann, B.P., and Woessner, J. (2012) Influence of pore-pressure on the event-size distribution of induced earthquakes. *Geophysical Research Letters*, **39** (9): L09302.

Bellahsen, N., and Daniel, J.M. (2005). Fault reactivation control on normal fault growth: an experimental study. *Journal of Structural Geology*, **27**(4), pp.769-780.

Bickle M.J. (2009) Geological carbon storage. *Nature Geoscience*, **2**, pp.815–818.

Burland, J.B. (1990) On the compressibility and shear strength of natural clays. *Geotechnique* **40**, pp.329-378.

Byerlee, J.D. (1978) Friction of rocks. *Pure Applied Geophysics,* **116**, pp.615–626.

Cappa, F., and Rutqvist, J. (2011) Modeling of coupled deformation and permeability evolution during fault reactivation induced by deep underground injection of CO_2. *International Journal of Greenhouse Gas Control*, **5**(2), pp.336-346.

Cesca, S., Grigoli, F., Heimann, S., Gonzalez, A., Buforn, E., Maghsoudi, S., Blanch, E., and Dahm, T. (2014) The 2013 September–October seismic sequence offshore Spain: a case of seismicity triggered by gas injection? *Geophysical Journal International*, **198**, pp.941–953.

Clarke, H., Eisner, L., Styles, P., and Turner, P. (2014) Felt seismicity associated with shale gas hydraulic fracturing: The first documented example in Europe. *Geophysical Research Letters*, **41**(23), pp.8308-8314.

Collettini, C., Chiaraluce, L., Pucci, S., and Barchi, M.R. (2005) Looking at fault reactivation matching structural geology and seismological data. Journal of Structural Geology, 27 (5), 937-942.

Crawford, B.R., Faulkner, D.R., and Rutter, E.H. (2008) Strength, porosity, and permeability development during hydrostatic and shear loading of synthetic quartz-clay fault gouge. *Journal of Geophysical Research*, **113**, B03207, doi:10.1029/2006JB004634.

Cuss, R.J., and Harrington, J.F. (2016) An experimental study of the potential for fault reactivation during changes in gas and porewater pressure. *International Journal of Greenhouse Gas Control*, **53**, pp.41-55. DOI: 10.1016/j.ijggc.2016.07.028

Cuss, R.J., Graham, C.C., Wiseall, A.C, and Harrington, J.F. (2016) Cyclic loading of an idealized clay-filled fault; comparing hydraulic flow in two clay gouges. *Geofluids*, **16**, pp.552-564. DOI: 10.1111/gfl.12175.

Cuss, R.J., Milodowski, A.E., Harrington, J.F. and Noy, D.J. (2009) Fracture transmissivity test of an idealised fracture in Opalinus Clay. *British Geological Survey Commissioned Report*, **CR/09/163**. 74pp.

Cuss, R.J., Harrington, J.F., Graham, C.C., and Noy, D.J. (2014[a]) Observations of Pore Pressure in Clay-rich Materials; Implications for the Concept of Effective Stress Applied to Unconventional Hydrocarbons. European Geosciences Union General Assembly 2014, EGU Division Energy, Resources & the Environment (ERE). *Energy Procedia*, **59**, pp.59-66; doi:10.1016/j.egypro.2014.10.349

Cuss, R.J., Harrington, J.F., Milodowski, A.E., and Wiseall, A.C. (2014[b]) Experimental study of gas flow along an induced fracture in Opalinus Clay. *British Geological Survey Commissioned Report*, **CR/14/051**. 79pp.

Cuss, R.J., Harrington, J.F., Sathar, S., Norris, S., and Talandier, J. (2017) The role of the stress-path and importance of stress history on the flow of water along faults; an experimental study. *Applied Clay Science*, 150, pp.282-292, https://dx.doi.org/10.1016/j.clay.2017.09.029

Cuss, R.J., Milodowski, A., and Harrington, J.F. (2011) Fracture transmissivity as a function of normal and shear stress: first results in Opalinus clay. *Physics and Chemistry of the Earth*. **36**, pp.1960-1971. DOI: 10.1016/j.pce.2011.07.080

Del Ventisette, C., Montanari, D., Sani, F., & Bonini, M. (2006) Basin inversion and fault reactivation in laboratory experiments. *Journal of Structural Geology*, **28**(11), 2067-2083.

Dubois, A., Odonne, F., Massonnat, G., Lebourg, T., and Fabre, R. (2002) Analogue modelling of fault reactivation: tectonic inversion and oblique remobilisation of grabens. *Journal of Structural Geology*, 24(11), 1741-1752.

Economides, M.J., and Ehlig-Economides, C.A. (2009) Sequestering Carbon Dioxide in a Closed Underground Volume. *Society of Petroleum Engineers*, Richardson, TX, SPE 124430.

Ellsworth, W.L. (2013) Injection-induced earthquakes. *Science*, **341**: 6142.

Faulkner, D.R., and Rutter, E.H. (2000) Comparisons of water and argon permeability in natural clay-bearing fault gouges under high pressure at 20 C. *Journal of Geophysical Research*, **105**, pp.16,415–16,426.

Faulkner, D.R., and Rutter, E.H. (2001) Can the maintenance of overpressured fluids in large strike-slip fault zones explain their apparent weakness? *Geology*, **29**, pp.503–506.

Gan, Q., and Elsworth, D. (2014) Analysis of fluid injection-induced fault reactivation and seismic slip in geothermal reservoirs. *Journal of Geophysical Research*, Solid Earth, **119**, pp.3340–3353, doi:10.1002/2013JB010679.

Gartrell, A., Lisk, M., and Underschultz, J. (2002) Controls on the trap intensity of the Skua Oil Field, Timor Sea. In: Keep, M and Moss, S. (Eds) The Sedimentary Basins of Wester Australia 3: Proceedings of the Petroleum Exploration society of Australia Symposium, Perth, WA, 389-407.

Gautschi, A. (2001) Hydrogeology of a fractured shale (Opalinus Clay): Implications for deep geological disposal of radioactive wastes. *Hydrogeology Journal*, **9**, pp.97–107

Haszeldine, R.S. (2009) Carbon capture and storage: How green can black be? *Science*, **325**(5948): pp.1647–1652.

Highley, D.E. (1984) China Clay. Mineral Dossier No. 26. Mineral Resources Consultative Committee, HMSO, London.

Holland, A. (2013) Earthquakes triggered by hydraulic fracturing in south-central Oklahoma, *Bull. Seismol. Soc. Am.*, **103**, pp.1784–1792.

Horseman, S., Winter, M., and Entwistle, D. (1987) Geotechnical characterisation of Boom Clay in relation to disposal of radioactive waste, Report EUR 10987, Luxembourg: Commission of the European Communities.

Hubbert, M.K. and Rubey, W.W. (1959) Role of fluid pressure in the mechanics of overthrust faulting. *Bull. geol. Soc. Am.*, **70**, pp.115-205

Krantz, R.W. (1991) Measurements of friction coefficients and cohesion for faulting and fault reactivation in laboratory models using sand and sand mixtures. *Tectonophysics*, **188**(1-2), pp.203-207.

Mathieson, A., Midgley, J., Dodds, K., Wright, I., Ringrose, P., and Saoul, N. (2010) CO_2 sequestration monitoring and verification technologies applied at Krechba, Algeria. *The Leading Edge*, **29**(2), pp.216-222.

Moeck, I., Kqiatek, G., and Zimmermann, G. (2009) Slip tendency analysis, fault reactivation potential and induced seismicity in a deep geothermal reservoir. Journal of Structural Geology, 31 (10), 1174-1182).

Morris, A., Ferrill, D.A., and Henderson, D.B. (1996) Slip-tendency analysis and fault reactivation. Geology, 24 (3), 275-278.

Morrow, C.A., Shi, L.Q. and Byerlee, J.D. (1982) Strain hardening and strength of clay-rich fault gouges. *Journal of Geophysical Research: Solid Earth*, **87**(B8), pp.6771-6780.

Morrow, C.A., Radney, B. and Byerlee, J.D. (1992) Frictional Strength and the Effective Pressure Law of Montmorillonite and lllite Clays. *International Geophysics*, **51**, pp.69-88.

Morrow, C.A., Moore, D.E. and Lockner, D.A. (2000) The effect of mineral bond strength and adsorbed water on fault gouge frictional strength. *Geophysical research letters*, **27**(6), pp.815-818.

Noy, D.J., Holloway, S., Chadwick, R.A., Williams, J.D.O., Hannis, S.A. and Lahann, R.W. (2012) Modelling large-scale carbon dioxide injection into the Bunter Sandstone in the UK Southern North Sea. *International Journal of Greenhouse Gas Control*, **9**, 220–233.

Richard, P., and Krantz, R. W. (1991) Experiments on fault reactivation in strike-slip mode. *Tectonophysics*, **188**(1), pp.117-131.

Roscoe KH, Schofield A, and Wroth CP (1958) On the yielding of soils. Geotechnique 1958;8: pp.22–53.

Rutter, E.H., Faulkner, D.R., and Burgess, R. (2012) Structure and geological history of the Carboneras Fault Zone, SE Spain: Part of a stretching transform fault system. Journal of Structural Geology, 45, 68-71.

Rutqvist J. (2012) The Geomechanics of CO2 Storage in Deep Sedimentary Formations. *Geotechnical and Geological Engineering*, **30**(3), 525-551.

Saffer, D.M. and Marone, C. (2003) Comparison of smectite-and illite-rich gouge frictional properties: application to the updip limit of the seismogenic zone along subduction megathrusts. *Earth and Planetary Science Letters*, **215**(1), pp.219-235.

Sathar, S., Reeves, H.J., Cuss, R.J., and Harrington, H.J. (2012) The role of stress history on the flow of fluids through fractures. *Mineralogical Magazine*. December 2012, Vol. **76**(8), pp.3165-3177. DOI: 10.1180/minmag.2012.076.8.30

Schofield, A., and Wroth, C.P. (1968) Critical state soil mechanics. London: McGraw-Hill, 1968. p. 310

Scholz, C.H. (1990) *The Mechanics of Earthquakes and Faulting*. Cambridge University Press, Cambridge, New York, Port Chester, Melbourne, Sydney.

Segall, P., and Rice, J.R. (1995) Dilatancy, compaction, and slip instability of a fluid-infiltrated fault, *Journal of Geophysical Research*, **100**(B11), pp.22,155–22,171, doi:10.1029/95JB02403.

Sibson, R.H. (1994) Crustal stress, faulting and fluid flow. *Geological Society, London, Special Publications*, **78**(1), pp.69-84.

Skempton, A.W. (1970) First-time slides in over-consolidated clays. *Geotechnique*, **20**, pp.320-324.

Tembe, S., Lockner, D.A. and Wong, T.F. (2010) Effect of clay content and mineralogy on frictional sliding behavior of simulated gouges: Binary and ternary mixtures of quartz, illite, and montmorillonite. *Journal of Geophysical Research: Solid Earth*, **115**(B3) doi:10.1029/2009JB006383

Terzaghi, K. (1943) *Theoretical Soil Mechanics*. New York, John Wiley.

Verdon, J.P., Kendall, J.M., Stork, A.L., Chadwick, R.A., White, D.J., and Bissell, R.C. (2013) Comparison of geomechanical deformation induced by megatonne-scale CO_2 storage at Sleipner, Weyburn, and In Salah. *Proceedings of the National Academy of Sciences*, **110**(30), E2762-E2771.

Vilarrasa, V., and Carrera, J. (2015) Geologic Carbon Storage Is Unlikely to Trigger Large Earthquakes and Reactivate Faults through Which CO_2 Could Leak. *P. Natl. Acad. Sci. USA*, **112**(19), 5938-5943.

Wilson, M., and Monea, M. (2004) IEA GHG Weyburn CO_2 monitoring & storage project. Summary report 2000-2004. Petroleum Technology Research Centre, Regina, SK, Canada.

Zoback, M.D., and Gorelick, S.M. (2012) Earthquake triggering and large-scale geologic storage of carbon dioxide. *Proc Natl Acad Sci* USA **109**(26), pp.10164–10168.

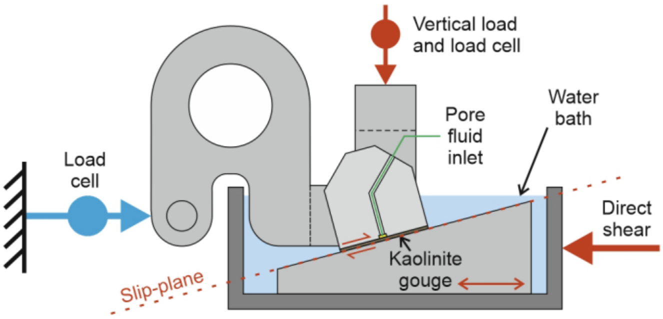

a

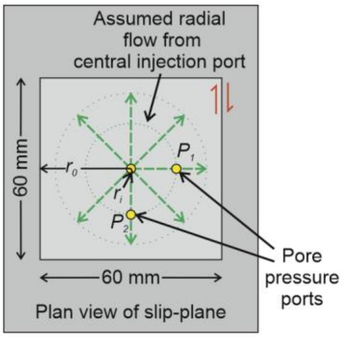

b

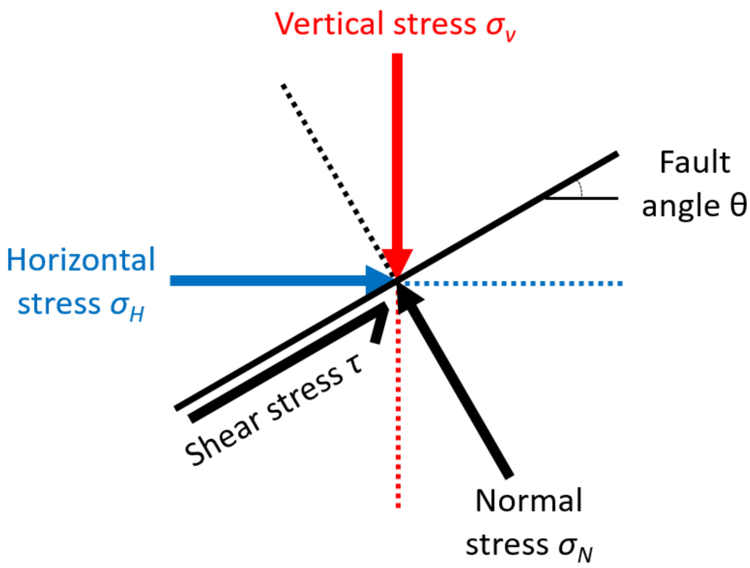

c

Figure 1 The Angled Shear Rig (ASR). a) Schematic of the apparatus; b) plan view of the slip-plane labelled in (a); c) Description of the stresses. Note that the apparatus directly measures vertical and horizontal stresses, whereas normal and shear stress were determined by stress rotation.

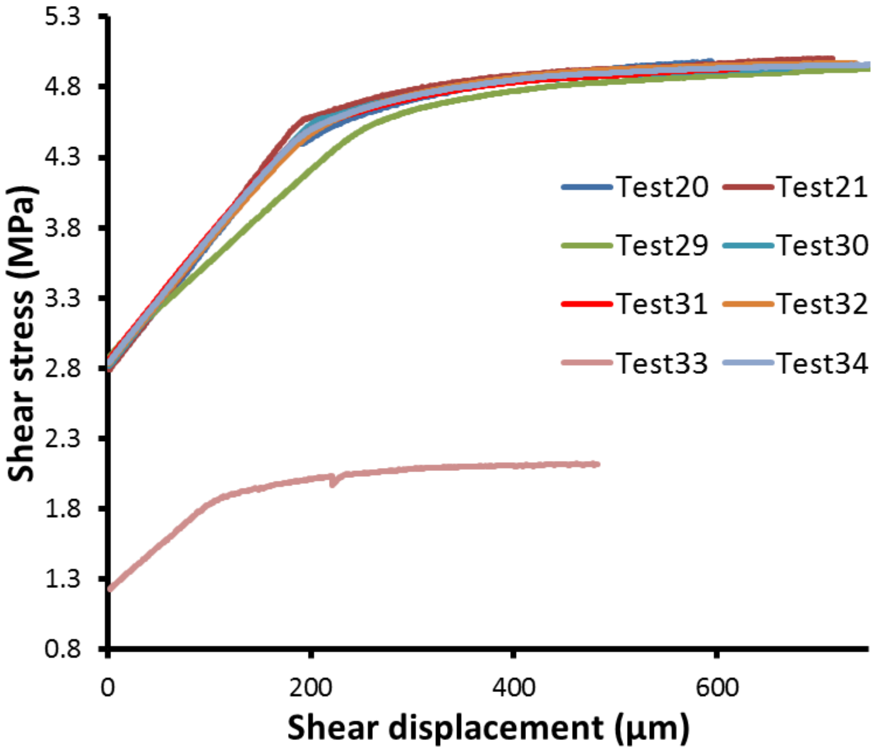

5.3
4.8
4.3
3.8
3.3
2.8
2.3
1.8
1.3
0.8
0
200
400
600
Shear stress (MPa)
Shear displacement (µm)
Test20
Test21
Test29
Test30
Test31
Test32
Test33
Test34

a

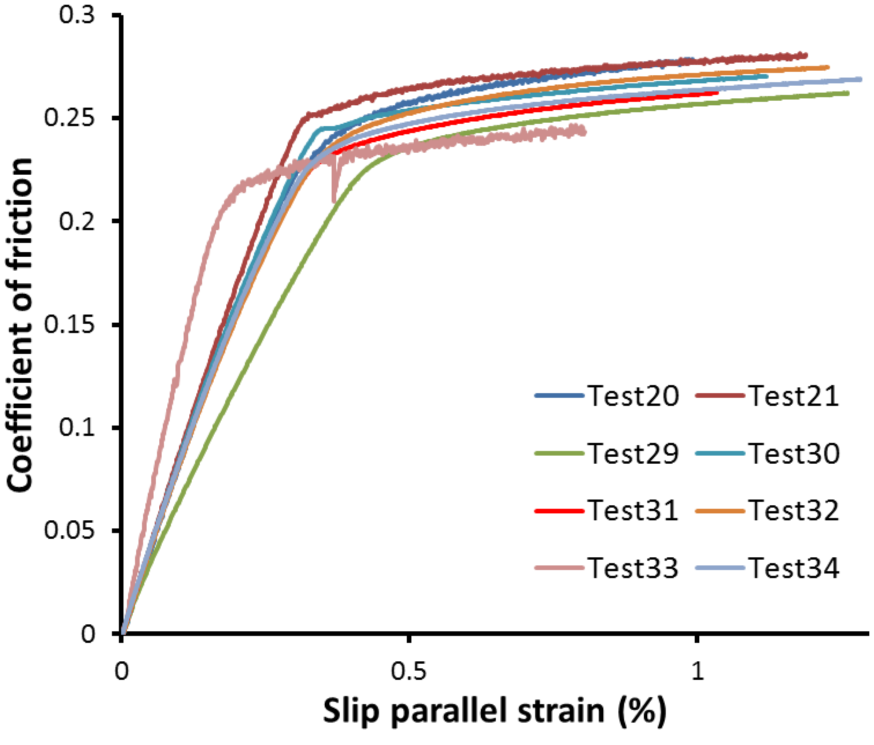

0.3
0.25
0.2
0.15
0.1
0.05
0
0
0.5
1
Coefficient of friction
Slip parallel strain (%)
Test20
Test21
Test29
Test30
Test31
Test32
Test33
Test34

b

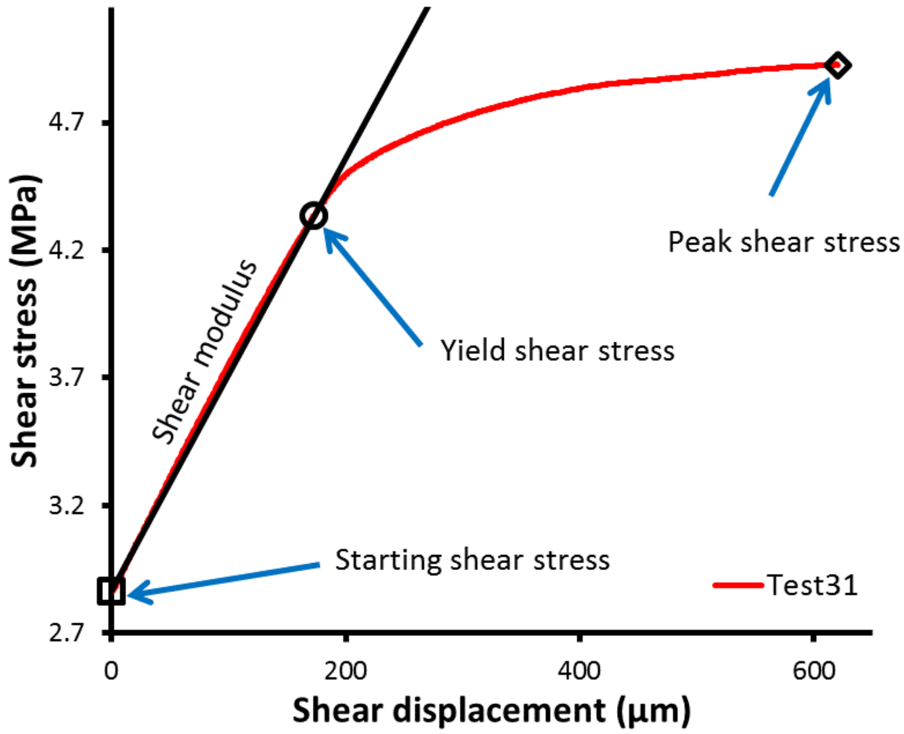

c

Figure 2 Mechanical strength data for shear tests conducted on kaolinite gouge material. a) Shear stress versus displacement; b) Variation of coefficient of friction during shear strain; c) Identification of starting shear stress, yield shear stress, peak shear stress, and shear modulus.

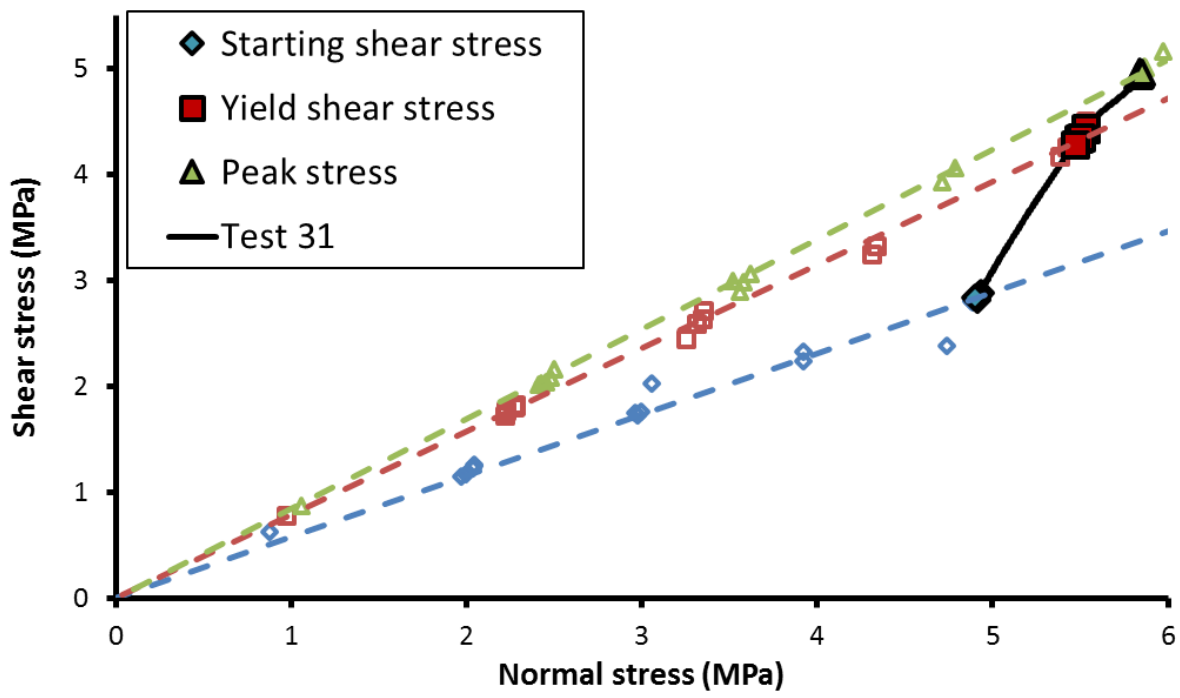

Figure 3 Strength parameters for shear tests conducted on kaolinite gouge. Clear linear trends are seen for the starting shear stress, the yield shear stress, and the peak shear stress. An example stress-strain result for test ASR_BigCCS_31Ksh. Note closed symbols are from the current study, open symbols are from Cuss & Harrington (2016).

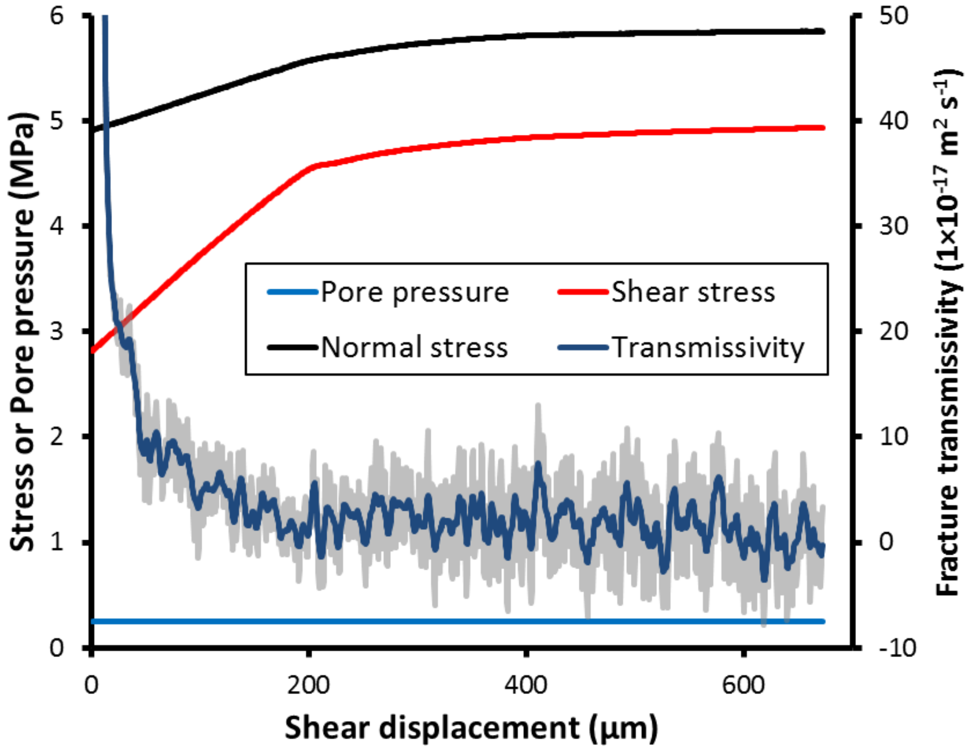

a

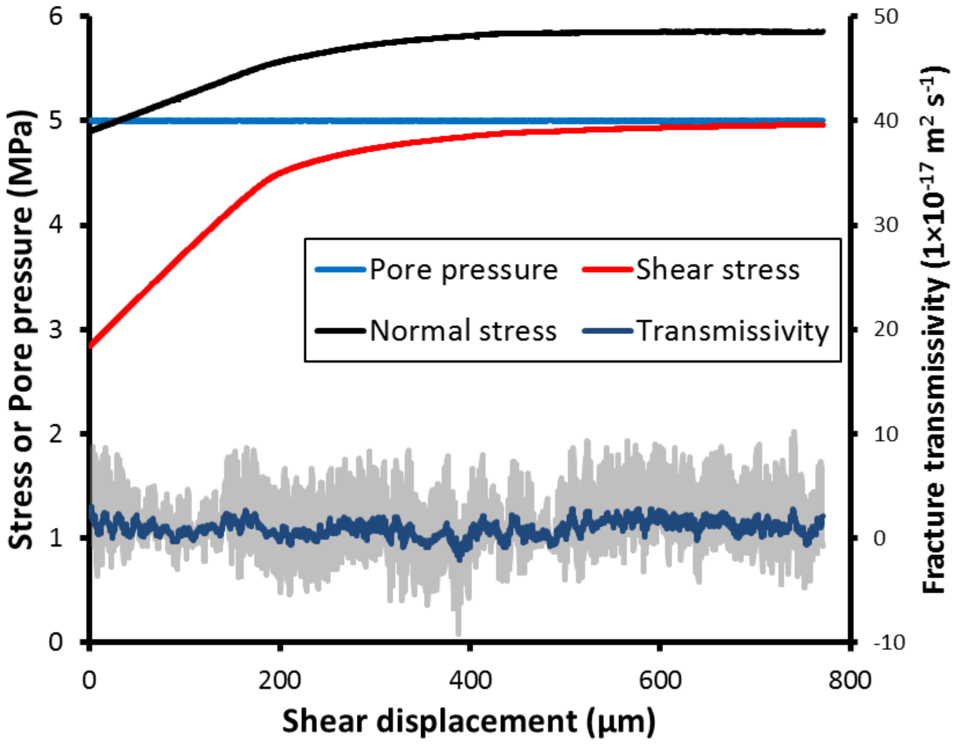

b

Figure 4 Flow variation during shearing for (a) test ASR_BigCCS_30Ksh; and (b) ASR_BigCCS_34Kfl. Fracture transmissivity is seen to reduce during test ASR_BigCCS_30Ksh (a), whereas it is low throughout test ASR_BigCCS_34Kfl (b).

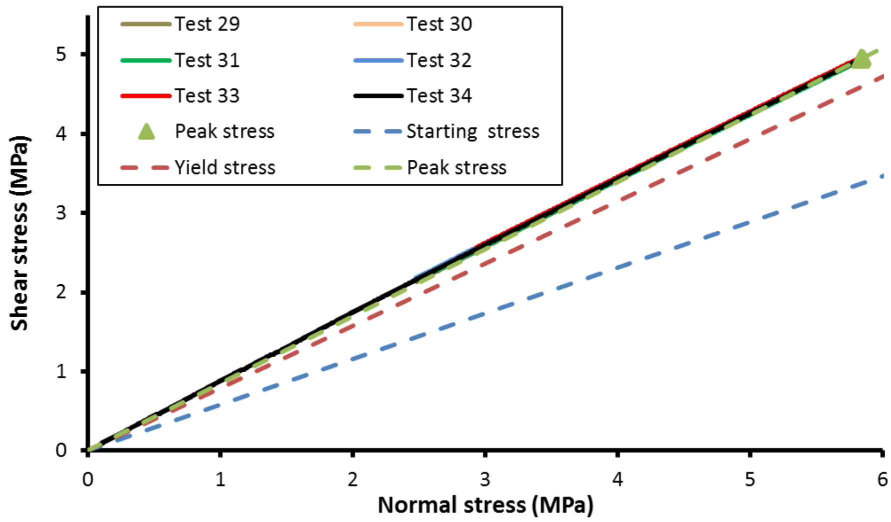

a

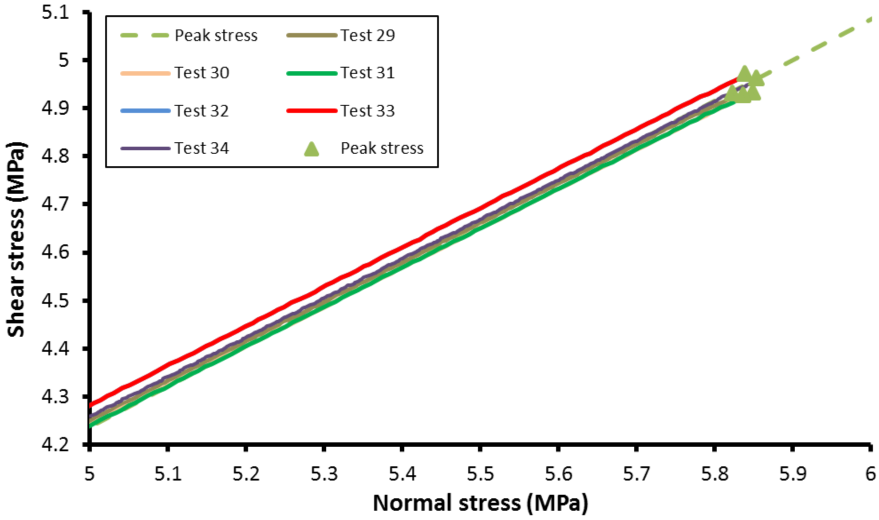

b

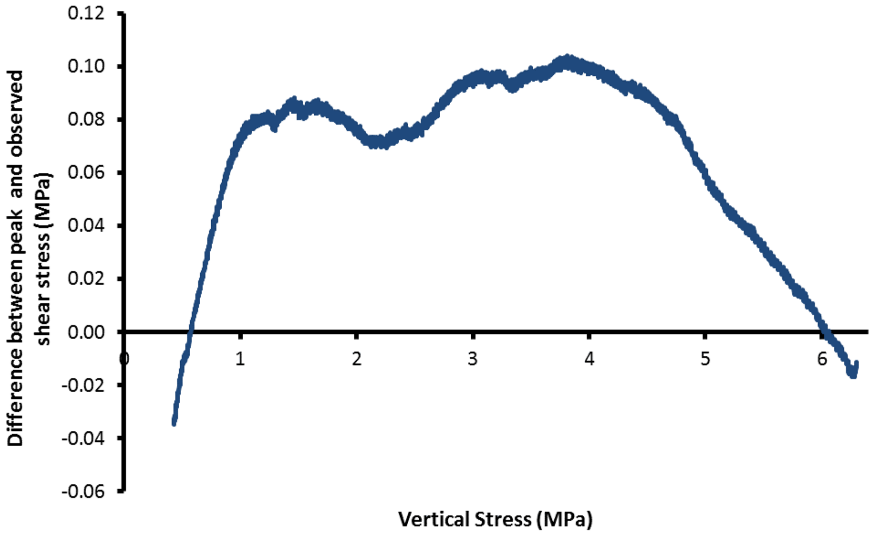

c

Figure 5 Mechanical response during fault unloading. All tests show that shear stress reduces in a manner parallel with the defined peak shear stress envelope (a, b). Close examination suggests a minor non-linearity of the data when comparing the observed shear stress with the peak stress envelope for test ASR_BigCCS_34Kfl (c).

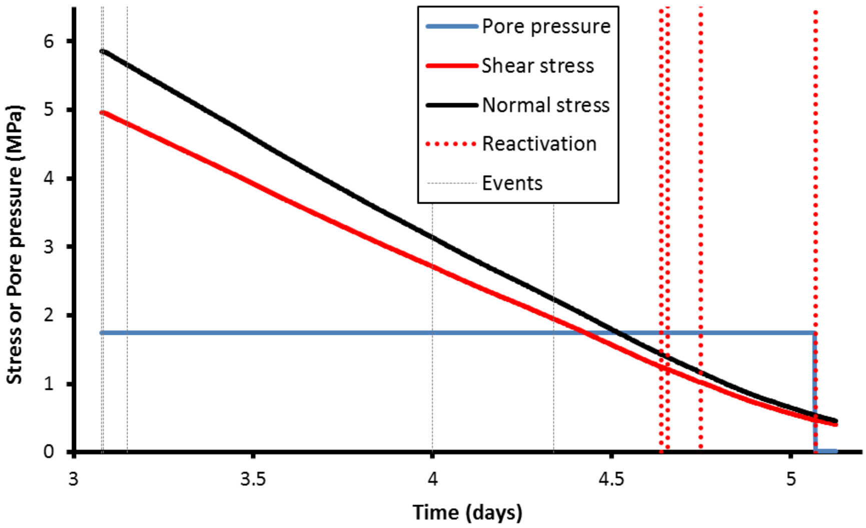
Pore pressure
Shear stress
Normal stress
Reactivation
Events
Stress or Pore pressure (MPa)
Time (days)

a

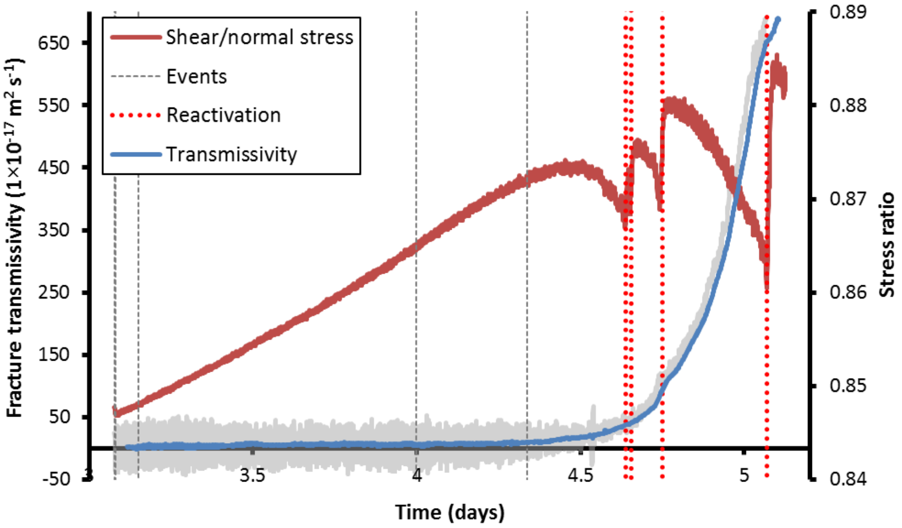
Shear/normal stress
Events
Reactivation
Transmissivity
Fracture transmissivity (1×10^{-17} m^2 s^{-1})
Stress ratio
Time (days)

b

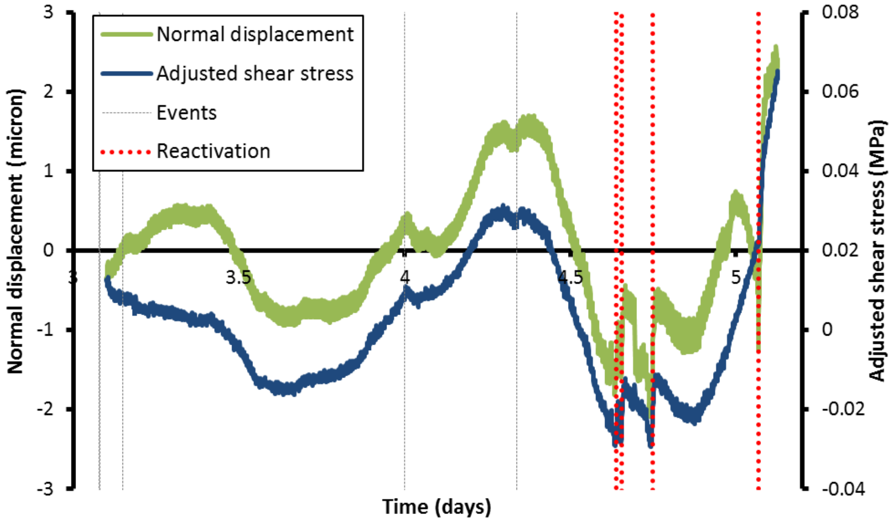
Normal displacement
Adjusted shear stress
Events
Reactivation
Normal displacement (micron)
Adjusted shear stress (MPa)
Time (days)

c

Figure 6 Data during vertical stress reduction stage of test ASR_BigCCS_34Kfl. a) normal stress, shear stress and average pore pressure during stress reduction; b) fracture transmissivity and ratio of shear to normal stress; c) normal displacement and adjusted shear stress (shear stress minus a polynomial).

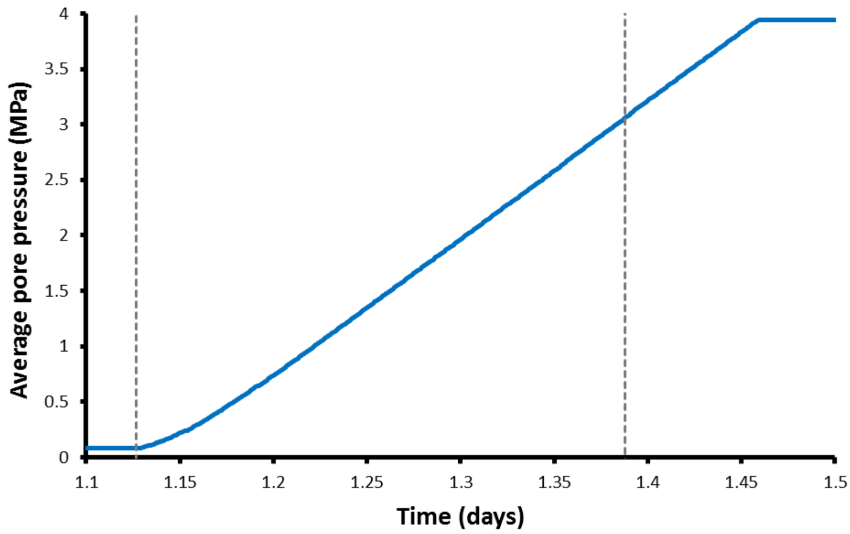
Average pore pressure (MPa)
4
3.5
3
2.5
2
1.5
1
0.5
0
1.1
1.15
1.2
1.25
1.3
1.35
1.4
1.45
1.5
Time (days)

A

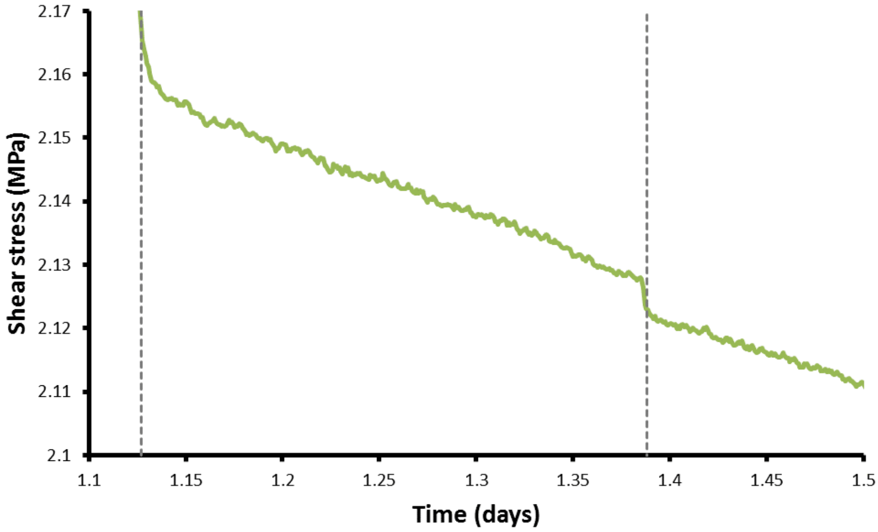
Shear stress (MPa)
2.17
2.16
2.15
2.14
2.13
2.12
2.11
2.1
1.1
1.15
1.2
1.25
1.3
1.35
1.4
1.45
1.5
Time (days)

B

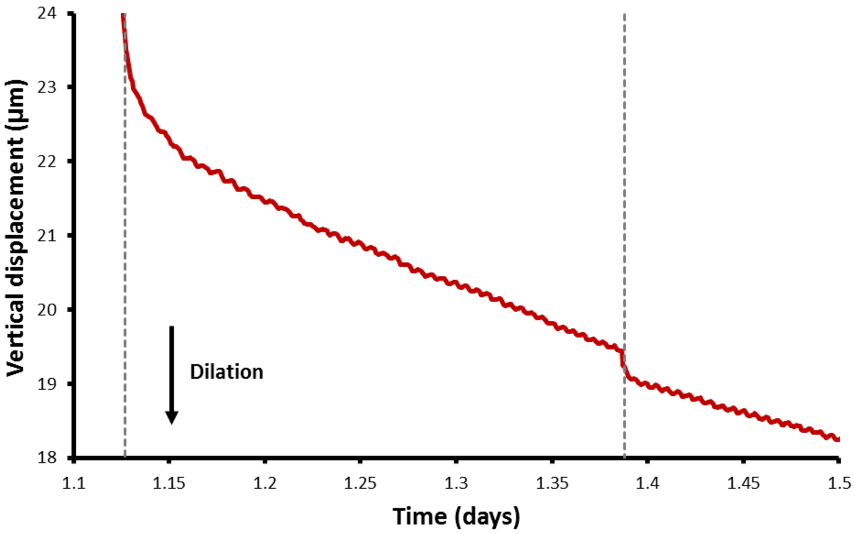
Vertical displacement (μm)
24
23
22
21
20
19
18
Dilation
1.1
1.15
1.2
1.25
1.3
1.35
1.4
1.45
1.5
Time (days)

C

Figure 7 Example results from fault reactivation test ASR_BigCCS_31Ksh. a) The injection of de-ionised water creates a pore pressure increase. Fault reactivation is identified by a reduction in shear stress (b) and vertical displacement on the fault plane (c).

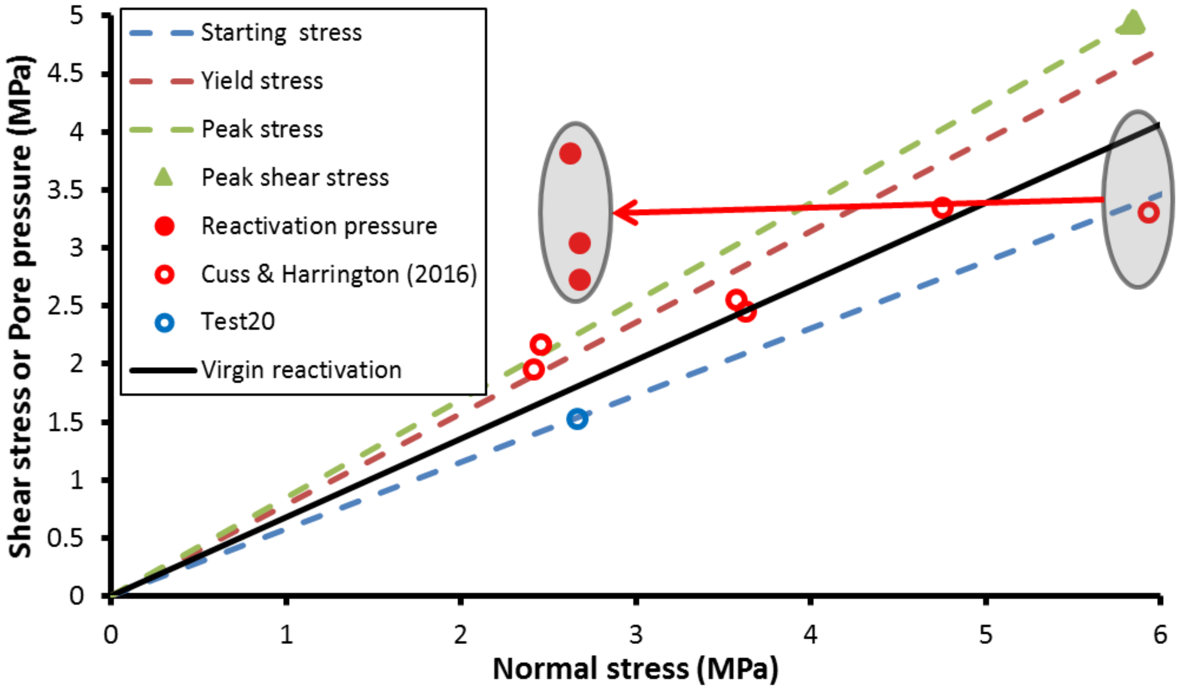

Figure 8 Results of fault slip following normal stress reduction. Results of the current study are compared with data without stress reduction (from Cuss & Harrington, 2016).

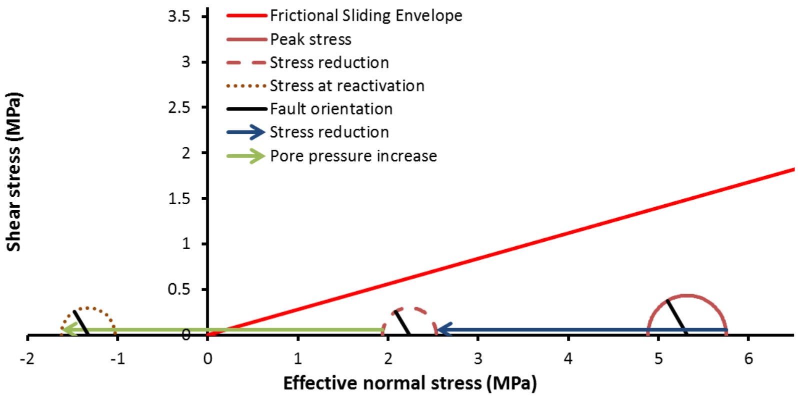

A

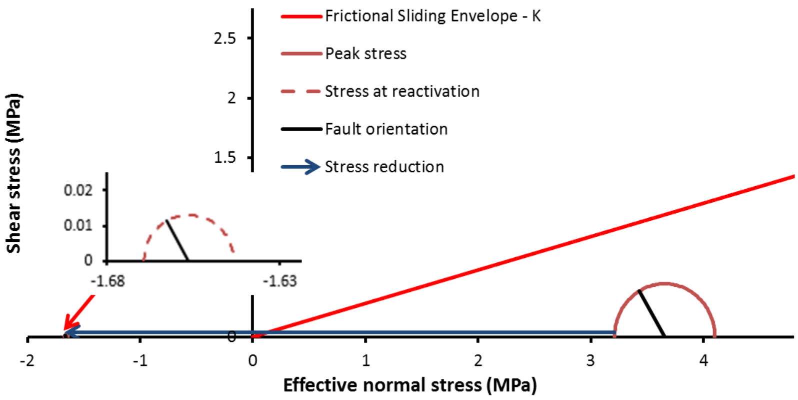

B

Figure 9 Mohr analysis of results from the current study. a) Stress-history test ASR_BigCCS_33Ksh, where stress has initially reduced as a result of the slow lowering of vertical stress, followed by a further effective stress reduction as pore pressure was increased in the fault gouge. b) Vertical stress reduction flow test ASR_BigCCS_34Kfl where effective stress was lowered until very low stress conditions, which due to the high pore pressure in the gouge greatly exceed the normal stress on the fault. greatly exceed the normal stress on the fault.

Experiment	Type of test	Normal (or Vertical) stress (MPa)					Shear (or Horizontal) stress (MPa)					Pore pressure during shear (MPa)	Reactivation pore-pressure (MPa)			Observation
		Average	Start	Yield	Peak	Reactivation	Shear modulus	Start	Yield	Peak	Reactivation		From maximum stress	From minimum stress	Observed	
ASR_BigCCS_20Kst	#1	4.87 (5.34)	4.88 (5.92)	5.43 (6.01)	5.84 (6.26)	2.67 (2.64)	461	2.81 (1.53)	4.26 (3.19)	4.98 (3.94)	2.65 (1.98)	0.50	3.91	1.65	1.53	Close to reduced stress condition
ASR_BigCCS_21Kfl	#2	5.63 (6.17)	4.88 (5.93)	5.53 (6.04)	5.88 (6.31)	/	497	2.79 (1.51)	4.50 (3.46)	5.00 (3.96)	/	0.25	3.95	/	/	Reactivation not observ
ASR_BigCCS_34Kfl		5.66 (6.21)	4.90 (5.93)	5.45 (6.06)	5.85 (6.30)	0.54 (0.58)	455	2.84 (1.57)	4.23 (3.14)	4.96 (3.91)	0.47 (0.43)	5.00	3.94	0.36	1.75	Reactivation not observ
ASR_BigCCS_29Ksh	#3	5.59 (6.16)	4.93 (5.96)	5.51 (6.08)	5.82 (6.27)	/	341	2.88 (1.61)	4.38 (3.30)	4.93 (3.89)	/	0.25	3.92	1.67	/	Reactivation not observ
ASR_BigCCS_30Ksh		5.62 (6.19)	4.91 (5.96)	5.50 (6.06)	5.85 (6.31)	2.50 (2.67)	454	2.82 (1.53)	4.39 (3.32)	4.93 (3.88)	2.15 (1.98)	0.25	3.95	1.67	2.73	Closer to maximum stre condition
ASR_BigCCS_31Ksh		5.60 (6.17)	4.92 (5.95)	5.48 (6.07)	5.84 (6.29)	2.49 (2.68)	441	2.86 (1.58)	4.30 (3.21)	4.93 (3.87)	2.12 (1.94)	0.25	3.93	1.68	3.05	Closer to maximum stre condition
ASR_BigCCS_32Ksh		5.64 (6.19)	4.91 (5.95)	5.48 (6.07)	5.84 (6.27)	/	437	2.83 (1.56)	4.30 (3.21)	4.97 (3.93)	/	0.25	3.92	1.66	/	Reactivation not observ
ASR_BigCCS_33Ksh		2.40 (2.59)	2.04 (2.43)	2.28 (2.48)	2.49 (2.67)	2.45 (2.62)	324	1.23 (0.78)	1.84 (1.52)	2.11 (1.97)	2.10 (1.92)	0.25	2.21	1.64	3.82	Greater than maximum stress condition

Table 1 – List of all experiments undertaken as part of the current study and corresponding results. #1 = stress history test with a stepped reduction in vertical stress; #2 = flow test during slow reduction in vertical stress to zero; #3 = stress history test with slow reduction in vertical stress; parenthesis indicate measured horizontal and vertical stresses.